Intensifying glycerol steam reforming on a monolith catalyst: a reaction kinetic model

L.F. Bobadilla[1], V. Blay[2], A. Álvarez [1,†], M.I. Domínguez[1], F. Romero-Sarria[1], M.A. Centeno[1,] and J.A. Odriozola[1]*

[1] Instituto de Ciencia de Materiales de Sevilla, Universidad de Sevilla-Consejo Superior de Investigaciones Científicas, Avenida Américo Vespucio s/n, 41092 Sevilla, España

[2] Instituto de Tecnología Química (UPV-CSIC), Universitat Politècnica de València, Consejo Superior de Investigaciones Científicas, Avenida de los Naranjos s/n, 46022 Valencia, España

AUTHOR INFORMATION

Corresponding Author

To whom correspondence should be addressed:

* Dr. Miguel A. Centeno (centeno@icmse.csic.es)

Present Addresses

[†] Institute of Chemical Research of Catalonia (ICIQ), The Barcelona Institute of Science and Technology, Av. Països Catalans 16, 43007 Tarragona, Spain

ABSTRACT. In this work, a structured monolithic catalyst has been tested under a wide range of conditions (partial pressure, residence time, temperature and time-on-stream), with the aim of modeling its kinetic behavior and assessing its economic and upscaling potential. We have developed a sequential model to help us interpret both main trends and salient features. Unexpected behavior was found for certain parameter

values, which led us to consider kinetic parasitic effects such as mass or heat transfer limitations. By independently invoking these effects, a conciliatory view of the results observed could not be reached. A combined explanation may prove successful, although overfitting could not be ruled out at this point. More importantly, however, the observed salient features of this stable and selective monolith catalyst may hold potential for process intensification of glycerol steam reforming, thus contributing to a more sustainable industry.

Keywords: *Ni monolith catalyst, kinetic modeling, mass and heat transfer*

1. Introduction

In recent years, biodiesel has attracted a considerable attention worldwide as an alternative renewable fuel to replace traditional petroleum diesel product because of limited reserves of traditional fossil resources, the instabilities of crude oil price and the concerns over greenhouse gases emissions [1, 2]. During the production of biodiesel by catalytic transesterification reaction from vegetable oils or animal fats, a large amount of glycerol is formed as byproduct. As a result of the increased biodiesel production during the last years, a saturated market for glycerol has provoked an expected fall in glycerol prices; therefore, finding effective and economical ways for conversion of glycerol into useful products is necessary. Recent studies have suggested that an attractive idea would be to produce hydrogen from glycerol via catalytic reforming processes, thus adding value to the glycerol surplus [3, 4].

Glycerol steam reforming (SR) has been demonstrated to be an effective method for hydrogen production with high selectivity, and it can be performed in gas or aqueous phase depending on the reaction conditions, mainly temperature and pressure [5]. Steam reforming, although highly endothermic, is preferable since the low pressure favours

selectivity to hydrogen. Nickel is the most used active metal for glycerol steam reforming because of its good activity for C-C, C-O and C-H bond cleavage, as well as for its ability to remove the adsorbed CO by water gas shift (WGS) reaction [6-17]. In addition to their optimal performance, Ni-based catalysts are preferred due to the low cost and high availability. However, the suppression of coke deposition to enhance catalytic stability still remains a major challenge. Different studies have suggested that the combination of basic promoters (Mg, Ce) and a group IV alloying element such as Sn favors coke-resistance of Ni catalysts in the SR of hydrocarbons [18-21]. Typically these additives help to avoid carbon deposition and enhance their catalytic stability.

In a previous paper [22], we demonstrated that a Ni-based monolith catalyst is very active and stable for hydrogen production by glycerol steam reforming. Coke formation was not observed in the monolith catalyst thanks to the strong interaction between the catalyst particles and the alumina layer in the monolith. The utilization of metallic monolith catalysts in practical applications is very important to control the heat and mass transport properties since the majority of catalytic reactions depend on heat transfer, fluid dynamics, and surface reaction kinetics. In addition to this, metallic monoliths are excellent models for the initial studies of microchannel reactors in which coupled endo- and exothermic reactions are used for controlling the process selectivity [23].

Concerning the reactor modeling, several studies on the kinetics and the reaction mechanism for glycerol steam reforming have been carried out in the last ten years [14, 24-27]. However, most of the reported kinetics are based on power-law models and refer to powdered catalysts. To the best of our knowledge, there are only two works published very recently that describe a kinetic model for glycerol steam reforming using a wall-coated catalytic microchannel [28] and a kinetic study of autothermal reforming

of glycerol in a dual layer monolith catalyst [29], respectively. Liu et al. found that the reaction rate of glycerol reforming was not limited by mass transfer within the catalyst washcoated layer and the surface reaction was the rate controlling step Langmuir-Hinshelwood kinetics considering non-dissociative adsorption of glycerol and dissociative adsorption of steam were proposed to describe the autothermal reforming of glycerol in this dual layer monolith catalyst [29].

This work involves a detailed study with the aim of understanding the kinetic behavior of the well-performing Ni-based monolith catalyst under a wider range of conditions (partial pressure, residence time, temperature and time-on-stream), looking out for potential upscaling. We anticipate that unusual effects were found in this study, which we attempted to rationalize based on the data at hand and prior knowledge. These results may well deserve additional work, as they hold promise for improved economics at commercial scale.

2. Experimental

2.1. Synthesis of NiSn/CeO_2-MgO/Al_2O_3 catalyst

NiSn/CeO_2-MgO/Al_2O_3 catalyst was prepared by the impregnation method using a synthesis procedure previously reported [19, 22]. Spherical pellets of γ-Al_2O_3 (*Spheralite SCS505*) with 2.5 mm diameter were milled in a high-energy ball mill in order to obtain γ-Al_2O_3 with a particle size of 7–8 μm, which was used as support to prepare the catalyst used in this study. All the precursors were impregnated simultaneously on the alumina support with an aqueous solution containing appropriate quantities of $Mg(NO_3)_2 \cdot 6H_2O$ (Sigma-Aldrich), $Ce(NO_3)_3 \cdot 6H_2O$ (Fluka), $Ni(NO_3)_2 \cdot 6H_2O$ (Panreac) and $SnCl_2$ anhydrous (Fluka), followed by drying overnight

at 120°C and final calcination in air at 700°C for 12 h. The nominal metal loading was 26 wt.% with a Ni-to-Sn atomic ratio equal to 6.

2.2. Metallic monolith manufacture

Metallic sheets of AluChrom YHf® with 50 μm thickness (Goodfellow) were used as substrates for preparation of the metallic monolith. Cylindrical monoliths were prepared by rolling flat and corrugated foils alternatively around a spindle (L = 30 mm, d = 16 mm, V = 6 cm^3, cell density 170 cells/cm^2), following the steps presented in Fig. 1. This geometry was optimized previously to ensure a more efficient heat and mass transfer [30-32], as will be discussed below. The metallic monolith was thermally pretreated in air at 900 ºC for 22 h in order to generate an adherent α-Al_2O_3 layer [33]. This treatment ensures a good adherence of the catalyst to the metallic substrate.

2.3.Washcoating process

The first requirement for an effective washcoating process is obtaining stable slurries. In order to achieve a uniform coating of the metallic substrate it is necessary to prepare the slurry controlling the parameters affecting its stability, such as particle size of the material to be dispersed, solid content of the suspension, pH and viscosity. Furthermore, the use of additives in the slurry formulation attempts to improve the catalyst adherence and the washcoat drying process. For instance, the addition of colloidal alumina (Nyacol, 20 wt% Al_2O_3), that presents a narrow particle size distribution, enhances remarkably the catalyst adherence owing to the smaller particles interlocking with the larger ones [34]. After several trials of slurry formulation for washcoating, we achieved a stable aqueous slurry of the catalyst previously prepared as described in section 2.1. The catalyst was milled in an agate mortar achieving an average particle size of 12.7 μm. Since the isoelectric point (IEP) of the catalyst is equal to 7.8, the pH was fixed at

3.5 using acetic acid to ensure high values of zeta potential, which translates into high repulsions between the particles and improved stability of the slurries. The following proportions of catalyst and colloidal alumina were selected: 61 wt% catalyst content and 39 wt% colloidal alumina, being the total solid content of the aqueous suspension ca. 24 wt%. The metallic monolith substrate was dipped into the slurry for 60 s, withdrawn at a constant speed of 3 cm min^{-1} and then the excess of suspension in the microchannels was removed by centrifugation at 500 rpm for 5 min. This procedure was repeated several times with intermediate drying steps at 120 C for 30 min between coatings until ca. 200 mg of the catalyst was deposited. Finally, the coated structured support was calcined at 700°C for 12 h. This procedure resulted in a catalyst loading on the monolith of 0.56 mg cm^{-2} after four washcoating steps. The adherence of the catalytic layer was evaluated with the ultrasound test [35] achieving a value better than 97%

2.4. Catalytic performance: stability test

The catalytic measurements were carried out in a computerized commercial Microactivity Reference catalytic reactor (PID Eng&Tech), employing a *Hastelloy C-276* tubular reactor (Autoclave Engineers) with 17 mm internal diameter, which contained the monolith loaded with 200 mg of catalyst. Prior to reaction, the catalyst was reduced *in situ* at 750°C for 1 h with 100 mL min^{-1} of H_2 (50%, v/v in inert). The experimental runs were conducted at 750 °C and atmospheric pressure with a steam-to-carbon ratio of 4 ($p_{steam} \approx 0.32$ atm; $p_G \approx 0.027$ atm) and 100 NL g^{-1} h^{-1} contact time in order to ensure an optimal catalytic activity [19]. At the reactor outlet a Peltier gas–liquid separator was fitted allowing the analysis of gas and liquid phase products separately. Gas products were analyzed on line using a microGC (Varian 4900) equipped with Porapak Q and MS-5A columns. Liquid products were analyzed by

HPLC (Varian 356-LC) equipped with a refractive index detector and a *Hi-Plex H* column with deionized water as eluent.

2.5. Kinetic measurements

Kinetic data for the glycerol steam reforming reaction were collected at atmospheric pressure and a reaction temperature of 600 ºC in order to achieve intermediate conversions. Glycerol-water mixtures with compositions ranging from 30 wt.% to 45 wt.% (corresponding to steam-to-carbon ratios of 1.7 to 4) were fed to ensure a stoichiometric excess of steam. This stream was diluted into flowing N_2 to yield steam partial pressures in the range p_{steam} = 0.11-0.32 atm. The resulting contact times employed in the experimental runs are thus between 100 and 230 NL g^{-1} h^{-1}. Thanks to the high cell density of the monolith designed, these translate into gas hourly space velocity (GHSV) values of 3500-7500 h^{-1}. High GHSV figures are interesting from an industrial point of view, as they would allow process intensification (PI) with more compact reactor designs. Results presented in this work correspond to a time-on-stream of 7 min, although the trends were found consistent with results after 1 h, and even much longer. At the industrial scale a higher temperature would be used to ensure a maximal conversion and catalytic stability such as 750 ºC (section 2.4).

2.6. Model simulation

As will be explained below, models used to help us in rationalizing the data comprise coupled differential and algebraic equations, namely property balances along with rate equations, which need to be solved simultaneously. To this end, models were implemented on Matlab 7.11.0 as custom made scripts. To solve them, we used the built-in solver *ode15s*. It is a variable-order solver based on numerical differentiation formulas. It was chosen because of its ability to deal with stiff problems, which we

anticipated that might arise if some of the pathways in the proposed reaction scheme lose relevance as optimization proceeds. On top of that, for parameter optimization, a high-level multistart procedure was used, repeating the optimization algorithm starting from different combinations of seed parameter values resulting from a logarithmic-factorial division of the parameter space. As for the optimization algorithm itself, we opted for the *fminsearch* routine in Matlab, which is a finely coded version of the classical Nelder-Mead algorithm. The objective function (O.F.) in such a minimization was designed to be:

$$O.F. = \sum \left[\left(F_{CO}^{exp} - F_{CO}^{calc} \right)^2 + \left(F_{H2}^{exp} - F_{H2}^{calc} \right)^2 \right] \quad \text{(Eq. 1)}$$

where the summation extends to all experiments performed. This was chosen on the basis that: 1) the rest of main products, namely H_2O and CO_2 were found to be stoichiometrically related to CO and H_2 based on the two main reactions presented below, and 2) both H_2 and CO are major products detected by the same GC detector, thus maximizing repeatability of measurements.

3. Results and discussion

3.1. Catalytic performance

In order to investigate the performance of the monolith catalyst for glycerol steam reforming, an initial experiment was performed at 750 °C employing a steam-to-carbon ratio of 4 and a space velocity of 100 NL g^{-1} h^{-1}. Fig. 2 shows that the monolithic catalyst exhibited good activity and stability in terms of hydrogen yield over 55 hours of time-on-stream. Only non-condensable products such as H_2, CO_2, CH_4 and CO were formed by glycerol steam reforming (Reaction (1)), glycerol decomposition (Reaction (2)) and WGS (Reaction (3)). Formation of CH_4 results from methanation reactions

(Reactions (4) and (5)) by coupling of H_2 and CO or CO_2 formed from glycerol decomposition.

$$C_3H_8O_3 + 3H_2O \rightarrow 3CO_2 + 7H_2 \quad (1)$$

$$C_3H_8O_3 \rightarrow 3CO + 4H_2 \quad (2)$$

$$CO + H_2O \leftrightarrow CO_2 + H_2 \quad (3)$$

$$CO + 3H_2 \leftrightarrow CH_4 + H_2O \quad (4)$$

$$CO_2 + 4H_2 \leftrightarrow CH_4 + 2H_2O \quad (5)$$

$$2CO \leftrightarrow CO_2 + C \quad (6)$$

As can be seen in Fig. 2, the CO-to-CO_2 molar ratio remains practically unaltered. This agrees with the absence of carbon deposits that could react with the CO_2 formed according to the Boudouard reaction (Reaction (6)) and alter the CO-to-CO_2 molar ratio as the reaction proceeds. In a previous report [22], we have investigated comprehensively the phenomena of deactivation by carbon deposition as a function of the catalyst shape for glycerol steam reforming reaction and we demonstrated that the formation of coke on the monolithic catalyst is minimized. These characteristics make this monolithic catalyst appropriate for an additional study of reaction kinetics.

3.2. Reaction kinetic model

Fig. 3 represents initial glycerol conversion to non-condensable products as a function of space time in the monolithic catalyst. Space time in this figure has been referred to the reaction temperature (600 °C) to be more suggestive of the short residence times actually used. Data points are labelled with partial pressures of the reactants in the feed

(glycerol, steam) with N_2 balance up to 1 atm. All results were obtained from the same monolithic catalyst by changing the individual reactants and inert flows. As one would expect, the general trend is an increase in glycerol conversion as contact time is increased. However, differences from the general trend can be readily identified both at short and long contact times. At short contact times, glycerol conversion decreases on increasing glycerol partial pressure, which would suggest a negative partial order with respect to glycerol under these conditions. In these experiments, steam partial pressure was maintained constant at 0.32 atm, and only glycerol partial pressure in the feed was modified. At long contact times it can also be seen a negative effect of glycerol partial pressure, although the effect seems different from that at shorter contact times.

Regarding the general trend, opposing results can be appreciated. On one hand, some data do not support a negative effect of glycerol partial pressure. If this were the case, as contact time is increased, data from a given glycerol partial pressure in the feed would exhibit a conversion deviating positively from a straight line (which would correspond to zero-order kinetics). By contrast, if one takes into consideration the points for a glycerol partial pressure in the feed of 0.017 atm (Fig. 3a, dashed line), the trends are compatible with a positive partial order with respect to glycerol kinetics, that is, deviating negatively from a straight line as contact time increases.

On the other hand, some data suggest a significant acceleration of the reaction kinetics when contact time is increased (Fig. 3b), which would indicate a negative partial order with respect to glycerol, as pointed out above. However, this may also be related to the multi-step nature of the glycerol reforming process (see below). Notice that since the steam partial pressure is in great stoichiometric excess, its effect may have reached saturation, and thus the partial order with respect to water can be assumed close

to zero in the discussion. Even if it had a strong influence, however, we still find opposing trends hard to conciliate.

From a ~~kinetic~~ modeling standpoint, one can propose several disturbing effects in order to explain the different observed trends. It is clear that as more phenomena are invoked the modeler has more degrees of freedom available to fit the data, although he can easily incur overfitting. Among these possible disturbances, we have selected to discuss three of them: CO_x formation as primary, secondary and/or tertiary products; unnoticed thermal effects, and some thoughts on hydrodynamics and mass transfer. According to Silva et al. [28], most of the kinetics studies for glycerol steam reforming refer to the glycerol consumption rather than to each of the reactions that normally take part in the process (glycerol thermal decomposition, WGS and methanation of carbon monoxide) or to each of the products that are formed (H_2, CO, CO_2 and CH_4). In this study we described our model using the WGS reaction and the glycerol thermal decomposition since the formation of methane or other by-products is negligible.

One may consider CO_x (CO and CO_2) to be not, or not only, primary products. For instance, glycerol may suffer some partial thermal decomposition to intermediate species precluding its steam reforming on the catalyst surface. Thus, one may consider CO_x to be a primary, secondary or tertiary product, or a combination thereof. Fig. 4 shows a simplified scheme in which steam reforming products can be formed as primary, secondary and tertiary products. This is reasonable with the fact that at short contact times some liquid products are detected (such as hydroxyacetone, 1,3-propanediol or glyceraldehyde), which would fall in some of the intermediate lumps proposed. According to this scheme, some steam reforming may occur on the starting glycerol, leading to CO_x formation at short space times. Simultaneously this glycerol may decompose into some intermediate species which are not so readily reformed,

therefore residing longer on the catalyst surface. Highly carbonaceous deposits, if any, would be captured into these intermediates lumps, which could eventually be gasified to reforming products in accordance with our previous work [22]. This would account for a decrease in the CO_x product formation rate. Finally, if residence time is long enough, these intermediates could be thermally decomposed into CO_x along with hydrogen, and/or into more easily reformable intermediate species, leading eventually to reforming products.

In our previous study [22], we found that glycerol is converted into condensable products and these are further reformed to carbon oxides and hydrogen following a sequential reaction scheme. At longer residence times, condensable products and coke formation diminish because they are gasified to gaseous products in the presence of steam. A similar behavior was observed by Iojoiu et al.[36] for the hydrogen production from biomass-derived pyrolysis oil using both Pt and Rh-based catalysts deposited on cordierite monoliths. They suggested an initial thermal cracking in which primary products such as H_2, CO_x, CH_4, C_nH_{n+2} and $C_xH_yO_z$ are formed. Afterwards, secondary catalytic reactions including steam cracking and/or steam reforming would take place on the active metal sites of the catalyst or at the metal–support interface, forming mainly CO_x and hydrogen.

A kinetic model was proposed in accordance with the scheme in Fig. 4. For this, first-order kinetics with respect to reactants were considered for each reaction step. Given the excess of water, its effect was included in the apparent kinetic constants, although it is made explicit in the water gas shift reaction rate. This reaction can be equilibrium limited (see below), and so the rate for the reverse water gas shift reaction is also considered: notice that in Eq. 7 K_p represents the equilibrium constant of the water gas

shift reaction, so that k_{WGS}/K_p is the kinetic constant of the reverse water gas shift reaction.

$$r_{dG} = k_{dG} \cdot p_G \quad \text{(Eq. 2)}$$

$$r_{rG} = k_{rG} \cdot p_G \quad \text{(Eq. 3)}$$

$$r_{rA} = k_{rA} \cdot p_A \quad \text{(Eq. 4)}$$

$$r_{dA} = k_{dA} \cdot p_A \quad \text{(Eq. 5)}$$

$$r_{rB} = k_{rB} \cdot p_B \quad \text{(Eq. 6)}$$

$$r_{WGS} = k_{WGS} \cdot p_{CO} \cdot p_{H2O} - \frac{k_{WGS}}{K_p} \cdot p_{CO2} \cdot p_{H2} \quad \text{(Eq. 7)}$$

$$\frac{dF_G}{dV} = -r_{rG} - r_{dG} \quad \text{(Eq. 8)}$$

$$\frac{dF_{H2O}}{dV} = -r_{WGS} \quad \text{(Eq. 9)}$$

$$\frac{dF_{CO}}{dV} = 3 \cdot r_{rG} + 3 \cdot r_{rA} + 3 \cdot r_{rB} - r_{WGS} \quad \text{(Eq. 10)}$$

$$\frac{dF_{H2}}{dV} = 4 \cdot r_{rG} + 4 \cdot r_{rA} + 4 \cdot r_{rB} + r_{WGS} \quad \text{(Eq. 11)}$$

$$\frac{dF_{CO2}}{dV} = r_{WGS} \quad \text{(Eq. 12)}$$

$$\frac{dF_{N2}}{dV} = 0 \quad \text{(Eq. 13)}$$

$$\frac{dF_A}{dV} = r_{dG} - r_{dA} - r_{rA} \quad \text{(Eq. 14)}$$

$$\frac{dF_B}{dV} = r_{dA} - r_{rB} \quad \text{(Eq. 15)}$$

The model presented takes into consideration the volume expansion associated with the stoichiometry of the reforming reaction. This is accounted for by differentiating the partial molar flows F_j instead of the partial pressures with respect to reaction volume. The relation between both can be obtained from the ideal gas model:

$$p_j = (F_j/\Sigma F_j) \cdot P \quad \text{(Eq. 16)}$$

Fig. 5 shows the solution to the above model where the parameters have been tuned manually to resemble the seat-shaped curves in Fig. 3. The model is not able to reproduce much more abrupt trends than those shown. Although the scheme proposed is in qualitative agreement with the seat-shaped curves displayed in Fig. 3b, it fails to explain the abrupt increase in conversion observed at longer space times. In particular, although an additional yield contribution at long space time can be rationalized, such an abrupt rise cannot be captured with simple kinetics. The later the reforming products are formed in the chain of reactions, the wider and softer its formation curve would appear as a function space time. An extreme example of this effect would be Fischer-Tropsch synthesis. In this case a large number of reactions in series prevent obtaining a sharp product distribution. For this reason, hydrocarbon chains are allowed to grow in excess, after which they may be selectively cracked down to achieve a cut with a sharper molecular weight distribution [37].

If the parameters are adjusted by means of an optimization algorithm considering all the data in Fig. 3, it is found that the possible secondary and/or tertiary origin of CO_x is disregarded (Fig. 6), which has to do with the trends in Fig. 3a and Fig. 3b opposing each other. Fig. 6 presents the parity plots obtained with the set of parameters adjusted by means of a multistart least-squares optimization algorithm. The optimal model converges to nearly first-order with respect to glycerol partial pressure, with deviations in conversions at the lower and higher ends in accordance to Fig. 3a.

In the literature other kinetic laws have been proposed to describe the catalyst behavior. Adhikari et al. [26] reported a kinetic modelling for glycerol steam reforming over Ni/CeO2. They estimated an activation energy of 103.4 kJ mol^{-1} using a power-law model that assumed a reaction order of 0.233 with respect to glycerol and zero-order with respect to steam. Sundari et al. [27] found a heterogeneous kinetic model that

suggests a first-order kinetics at low glycerol partial pressures for glycerol steam reforming using Ru/Al_2O_3. Cheng et al.[24] described single- and dual-site adsorption based on the Langmuir-Hinshelwood and Eley-Rideal rate expressions for glycerol steam reforming over $Co–Ni/Al_2O_3$. They found that a Langmuir–Hinshelwood mechanism with a rate-controlling step between glycerol and steam adsorbing on two different sites provides the most adequate representation. More recently, Silva et al. [28] have developed a phenomenological model that describes the glycerol steam reforming reaction in a packed bed reactor for predicting both glycerol consumption and products/by-products formation. They concluded that higher temperatures, higher water-to-glycerol feed ratios and higher pressures are more advantageous in terms of glycerol conversion and H_2 production.

In this work, H_2 yields were found to match up closely with the glycerol steam reforming reaction stoichiometry (Reaction (1)). This is interesting considering the possible lumps of intermediates before actual steam reforming (Fig. 4) or a possible coke deposition. In fact, glycerol C/H/O proportions are preserved in the gas and liquid phases, which would suggest a similar reactivity of compounds in intermediate lumps, if any, and does not support any extensive deposit of carbonaceous species on the monolith, in agreement with visual inspection after reaction.

To assess whether the monolith studied can be influencing the extent of the WGS reaction, we computed the approach to equilibrium for the different glycerol conversions, Γ_{WGS}:

$$\Gamma_{WGS} = \frac{p_{CO2} \cdot p_{H2}}{p_{CO} \cdot p_{H2O}} \frac{1}{K_p} \qquad \text{(Eq. 17)}$$

where K_p is the equilibrium constant in reaction (3), which can be estimated by Callaghan's equation [38] neglecting the fugacity coefficients for being close to unity:

$$log_{10}K_P = -2.4198 + 0.0003855\,T + 2180.6\,T^{-1} \quad \text{(Eq. 18)}$$

In Fig. 7, the approach to equilibrium for all data points in Fig. 3 is represented as a function of glycerol conversion to reforming products. Notice that as glycerol is initially reformed on the catalyst it does not yield a product mixture in equilibrium. However, in Fig. 7 a clearly evolving trend can be discerned, which would be in accordance with some involvement of the catalyst in the WGS reaction.

3.3. Heat and mass transfer limitations

Regarding Fig. 3b, one may think of other explanations for these trends, such as the possibility of a thermal runaway occurring at longer space times. In this case, as the conversion exceeds some threshold value, the heat released by the reaction may not be readily exchanged through the monolith walls, thus leading to heating and self-acceleration of the reaction. In spite of the moderate reaction enthalpy (-265 kJ mol^{-1}), given the high dilution of the reactant, good thermal conductivity (18 W m^{-1} K^{-1}) and high cell density (170 cells cm^{-2}) of the metallic monolith support, an unnoticed hot spot is unlikely to be a problem. Moreover, transient results during reactor startup do not show an increase of conversion with TOS or any change of the furnace temperature or its wattage.

Nevertheless, conventional rate equations do not suffice to explain the observed behavior, as was seen in Fig. 5. Another possibility is that the reactant mixture does not enter the monolith sufficiently hot, and thus part of the monolith behaves as a heat

exchanger, operating at a limited reaction rate. Only towards its end the gas mixture would reach the actual monolith temperature, potentially leading to a double improvement as contact time is increased. To inspect this possibility we developed an alternative model in which heat transfer will be assumed proportional to the temperature difference between the monolith and the fluid:

$$\frac{dT_{fluid}}{dV} = \kappa \cdot (T_{monolith} - T) \qquad \text{(Eq. 19)}$$

Notice that in this case the proportionality constant would depend notably on the flow, although it can be taken as a constant to simulate an approximated profile under given experimental conditions. In this line, to reduce the number of parameters depending on temperature, glycerol consumption rate was simplified down to a first order reaction, whose kinetic constant depends exponentially on temperature:

$$\frac{dF_G}{dV} = -k_{dG,873} \cdot exp\left(-\frac{E_{adG}}{R}\left(\frac{1}{T} - \frac{1}{873.15}\right)\right) \cdot p_G \qquad \text{(Eq. 20)}$$

For this simulation we assumed a relatively high activation energy of 110 kJ mol^{-1} as a worst-case scenario. Additionally, the equilibrium constant for the WGS is also highly temperature dependent (Eq. 18). One can observe that these kinetics lead to a relatively soft evolution of the temperature and concentration profiles (Fig. 8) and, consequently, they alone cannot explain the abrupt trends observed in Fig. 3b. Interestingly, by comparing the CO-to-CO_2 ratio in Figs. 5 and 8 one can notice, however, that there are differences: it is even possible to observe a maximum in the CO yield along the catalyst in the latter figure due to the reversibility of the WGS reaction, thus emphasizing the importance of temperature control if hydrogen yields are to be maximized, more so in

commercial scale operations where such thermal effects are easier to occur inadvertently.

Another effect that deserves consideration is the hydrodynamic behavior of the system. So far, we have based our discussion on pseudohomogeneous kinetics, i.e. by analogy to reactions in homogeneous media. However, the catalyst is heterogeneous, and therefore its activity is limited to the surface of its channels. In particular, reactants have to diffuse to the monolith surface, and products need to counterdiffuse back to the bulk gas phase (Fig. 9). The ease of this transport is affected by the bulk velocity of the fluid stream, affecting the effective thickness of the boundary layer next to the catalyst. On a more macroscopic scale, Reynolds number, impinging on axial and radial dispersion, will also affect the gas velocity profile to some extent. However, these transport coefficients are related to the fluid velocity with power-laws, whose exponents usually take values lower than 1 [39]. In addition, notice that the range of flows studied is far shorter than an order of magnitude and still marked differences have been observed. Given that temperature differences, which (approximately) follow a law of direct proportionality (i.e. a power to the unity, Eq. 19) and which affect exponentially the reaction rate constants cannot explain some of the abrupt changes observed, it is unlikely that mass transport limitations could provide more marked dependencies.

As has been discussed, in spite of the relatively limited parametric space swept in this study, a non-monotonic trend has already been observed. This makes data hard to interpret even when physical effects are accounted for (diffusion, dispersion, temperature). A combination of effects might certainly offer an explanation, although would require more extensive studies to avoid overfitting. Alternatively, it may well be that an additional, unaccounted effect is influencing the results. In either case, these trends are certainly worth further study since, as illustrated in Fig. 3b, could enable

dramatic improvements in terms of catalyst activity, allowing interesting options for process intensification. It is expected that *post-mortem* characterization after each reaction cycle along with *operando* studies of the catalyst surface will allow identifying the particularly active catalytic center for the glycerol steam reforming reaction and understanding the intrinsic reaction mechanism, yet maintaining the remarkable selectivity and stability of the present monolith, fostering in this way the industrial realization of this important process.

4. Conclusions

We have developed models to interpret the behavior of a Ni-based monolithic catalyst in the glycerol steam reforming reaction. A heterogeneous kinetic model based on a sequential reaction scheme presented reasonable adherence to the experimental results. However, an unexpected behavior was encountered for certain parameter values, which cannot be explained by conventional kinetic parasitic effects such as catalyst surface saturation or thermal runaway. This behavior deserves further investigation as it may unravel better-performing catalysts for glycerol steam reforming, a process holding great industrial interest.

NOMENCLATURE AND ABBREVIATIONS

Variables, parameters and constants

d	*Monolith external diameter* / cm
Ea	*Activation energy* / kJ mol^{-1}
F	*Molar flow* / mol s^{-1}
GHSV	*Gas hourly space velocity* (total flow, 0 °C, 1 atm) / h^{-1}
k	*Kinetic constant* / mol s^{-1} m^{-3} atm^{-1} or mol s^{-1} m^{-3} atm^{-2}

K_P	*Equilibrium constant* / -
L	*Monolith length* / cm
p	*Partial pressure* / atm
P	*Total pressure* / atm
r	*Reaction rate* / mol s^{-1} m^{-3}
R	*Universal gases constant* / J mol^{-1} K^{-1}
T	*Temperature* / °C
κ	*Modified global heat transfer coefficient* / cm^{-3}
V	*Monolith volume* / cm^3
Γ	*Approach to equilibrium* / -
τ	*Space time* / s

Subscripts

j	*j^{th} component*
0	*Initial*
A	*Lump A*
B	*Lump B*
d	*Thermal decomposition*
G	*Glycerol*
r	*Steam reforming*
WGS	*Water gas shift*

ACKNOWLEDGMENTS

The authors gratefully acknowledge the financial assistance from the Spanish Ministerio de Economía y Competitividad – MINECO (ENE2013-47880-C3-2-R and ENE2015-66975-C3-2-R) co-financed by FEDER funds from the European Union. L.

F. Bobadilla thanks the “Junta de Andalucía” for his fellowship with the project POG-TEP01965. V. Blay thanks the support from the Valencian Ministry of Education.

REFERENCES

[1] G. Baskar, R. Aiswarya, Trends in catalytic production of biodiesel from various feedstocks, Renew. Sustain. Energy Rev. 57 (2016) 496-504.

[2] D.M. Marinković, M.V. Stanković, A.V. Veličković, J.M. Avramović, M.R. Miladinović, O.O. Stamenković, V.B. Veljković, D.M. Jovanović, Calcium oxide as a promising heterogeneous catalyst for biodiesel production: Current state and perspectives, Renew. Sustain. Energy Rev. 56 (2016) 1387-1408.

[3] J.M. Silva, M.A. Soria, L.M. Madeira, Challenges and strategies for optimization of glycerol steam reforming process, Renew. Sustain. Energy Rev. 42 (2015) 1187-1213.

[4] B. Dou, Y. Song, C. Wang, H. Chen, Y. Xu, Hydrogen production from catalytic steam reforming of biodiesel byproduct glycerol: Issues and challenges, Renew. Sustain. Energy Rev. 30 (2014) 950-960.

[5] P.R.d.l. Piscina, N. Homs, Use of biofuels to produce hydrogen (reformation processes), Chem. Soc. Rev. 37 (2008) 2459-2467.

[6] S. Shao, A.-W. Shi, C.-L. Liu, R.-Z. Yang, W.-S. Dong, Hydrogen production from steam reforming of glycerol over Ni/CeZrO catalysts, Fuel Process. Technol. 125 (2014) 1-7.

[7] E. Gallegos-Suárez, F.R. García-García, I.D. González-Jiménez, I. Rodríguez-Ramos, A. Guerreo-Ruiz, K. Li, Ceramic hollow fibres catalytic enhanced reactors for glycerol steam reforming, Catal. Today 233 (2014) 21-30.

[8] E.A. Sanchez, R.A. Comelli, Hydrogen production by glycerol steam-reforming over nickel and nickel-cobalt impregnated on alumina, Int. J. Hydrogen Energy 39 (2014) 8650-8655.

[9] K. Seung-hoon, J. Jae-sun, Y. Eun-hyeok, L. Kwan-Young, M. Dong Ju, Hydrogen production by steam reforming of biomass-derived glycerol over Ni-based catalysts, Catal. Today 228 (2014) 145-151.

[10] M.L. Dieuzeide, V. Iannibelli, M. Jobbagy, N. Amadeo, Steam reforming of glycerol over Ni/Mg/γ-Al_2O_3 catalysts. Effect of calcination temperatures, Int. J. Hydrogen Energy 37 (2012) 14926-14930.

[11] M.L. Dieuzeide, M. Jobbagy, N. Amadeo, Glycerol steam reforming over Ni/γ-Al_2O_3 catalysts, modified with Mg(II). Effect of Mg (II) content, Catal. Today 213 (2013) 50-57.

[12] E.A. Sanchez, R.A. Comelli, Hydrogen by glycerol steam reforming on a nickel–alumina catalyst: Deactivation processes and regeneration, Int. J. Hydrogen Energy 37 (2012) 14740-14746.

[13] V.V. Thyssen, T.A. Maia, E.M. Assaf, Ni supported on La_2O_3–SiO_2 used to catalyze glycerol steam reforming, Fuel 105 (2013) 358-363.

[14] C.K. Cheng, S.Y. Foo, A.A. Adesina, Steam reforming of glycerol over Ni/Al_2O_3 catalyst, Catal. Today 178 (2011) 25-33.

[15] V. Nichele, M. Signoretto, F. Menegazzo, A. Gallo, V. Dal Santo, G. Cruciani, G. Cerrato, Glycerol steam reforming for hydrogen production: Design of Ni supported catalysts, Appl. Catal. B Environ. 111–112 (2012) 225-232.

[16] F. Pompeo, G.F. Santori, N.N. Nichio, Hydrogen production by glycerol steam reforming with Pt/SiO_2 and Ni/SiO_2 catalysts, Catal. Today 172 (2011) 183-188.

[17] I.N. Buffoni, F. Pompeo, G.F. Santori, N.N. Nichio, Nickel catalysts applied in steam reforming of glycerol for hydrogen production, Catal. Commun. 10 (2009) 1656-1660.

[18] A. Iriondo, V.L. Barrio, J.F. Cambra, P.L. Arias, M.B. Guemez, M.C. Sanchez-Sanchez, R.M. Navarro, J.L.G. Fierro, Glycerol steam reforming over Ni catalysts supported on ceria and ceria-promoted alumina, Int. J. Hydrogen Energy 35 (2010) 11622-11633.

[19] L.F. Bobadilla, A. Penkova, A. Álvarez, M.I. Domínguez, F. Romero-Sarria, M.A. Centeno, J.A. Odriozola, Glycerol steam reforming on bimetallic NiSn/CeO_2–MgO–Al_2O_3 catalysts: Influence of the support, reaction parameters and deactivation/regeneration processes, Appl. Catal. A Gen. 492 (2015) 38-47.

[20] L.F. Bobadilla, A. Penkova, F. Romero-Sarria, M.A. Centeno, J.A. Odriozola, Influence of the acid–base properties over NiSn/MgO–Al_2O_3 catalysts in the hydrogen production from glycerol steam reforming, Int. J. Hydrogen Energy 39 (2014) 5704-5712.

[21] J.W. Shabaker, G.W. Huber, J.A. Dumesic, Aqueous-phase reforming of oxygenated hydrocarbons over Sn-modified Ni catalysts, J. Catal. 222 (2004) 180-191.

[22] L.F. Bobadilla, A. Álvarez, M.I. Domínguez, F. Romero-Sarria, M.A. Centeno, M. Montes, J.A. Odriozola, Influence of the shape of Ni catalysts in the glycerol steam reforming, Appl. Catal. B Environ. 123–124 (2012) 379-390.

[23] G. Arzamendi, P.M. Diéguez, M. Montes, J.A. Odriozola, E. Falabella Sousa-Aguiar, L.M. Gandía, Computational fluid dynamics study of heat transfer in a microchannel reactor for low-temperature Fischer–Tropsch synthesis, Chem. Eng. J. 160 (2010) 915-922.

[24] C.K. Cheng, S.Y. Foo, A.A. Adesina, Carbon deposition on bimetallic Co–Ni/Al_2O_3 catalyst during steam reforming of glycerol, Catal. Today 164 (2011) 268-274.

[25] G.S. Go, H.J. Lee, D.J. Moon, Y.C. Kim, Glycerol steam reforming over Ni–Fe–Ce/Al_2O_3 catalyst for hydrogen production, Res. Chem. Intermed. 42 (2015) 289-304.

[26] S. Adhikari, S.D. Fernando, A. Haryanto, Kinetics and Reactor Modeling of Hydrogen Production from Glycerol via Steam Reforming Process over Ni/CeO_2 Catalysts, Chem. Eng. Technol. 32 (2009) 541-547.

[27] R. Sundari, P.D. Vaidya, Reaction Kinetics of Glycerol Steam Reforming Using a Ru/Al_2O_3 Catalyst, Energy & Fuels 26 (2012) 4195-4204.

[28] J.M. Silva, M.A. Soria, L.M. Madeira, Steam reforming of glycerol for hydrogen production: Modeling study, Int. J. Hydrogen Energy 41 (2016) 1408-1418.

[29] Y. Liu, A. Lawal, Kinetic study of autothermal reforming of glycerol in a dual layer monolith catalyst, Chem. Eng. Process. 95 (2015) 276-283.

[30] L.C. Almeida, F.J. Echave, O. Sanz, M.A. Centeno, G. Arzamendi, L.M. Gandía, E.F. Sousa-Aguiar, J.A. Odriozola, M. Montes, Fischer–Tropsch synthesis in microchannels, Chem. Eng. J. 167 (2011) 536-544.

[31] L.C. Almeida, F.J. Echave, O. Sanz, M.A. Centeno, J.A. Odriozola, M. Montes, Washcoating of metallic monoliths and microchannel reactors, in: E.M. Gaigneaux, M. Devillers, S. Hermans, P.A. Jacobs, J.A. Martens, P. Ruiz (Eds.) Stud. Surf. Sci. Catal. Elsevier 2010, pp. 25-33.

[32] O. Sanz, F.J. Echave, F. Romero-Sarria, J.A. Odriozola, M. Montes, Chapter 9 - Advances in structured and microstructured catalytic reactors for hydrogen production - Gandía, Luis M, in: G. Arzamendi, P.M. Diéguez (Eds.) Renew. Hydrogen Technol. Elsevier, Amsterdam, 2013, pp. 201-224.

[33] D.M. Frías, S. Nousir, I. Barrio, M. Montes, L.M. Martínez T, M.A. Centeno, J.A. Odriozola, Nucleation and growth of manganese oxides on metallic surfaces as a tool to prepare metallic monoliths, Appl. Catal. A Gen. 325 (2007) 205-212.

[34] T.A. Nijhuis, A.E.W. Beers, T. Vergunst, I. Hoek, F. Kapteijn, J.A. Moulijn, Preparation of monolithic catalysts, Catal. Rev. 43 (2001) 345-380.

[35] K.Ohkubo, Y.Y.S. Yasaki, United States Patent, 1993. Patent number 5 208 206

[36] E.E. Iojoiu, M.E. Domine, T. Davidian, N. Guilhaume, C. Mirodatos, Hydrogen production by sequential cracking of biomass-derived pyrolysis oil over noble metal catalysts supported on ceria-zirconia, Appl. Catal. A Gen. 323 (2007) 147-161.

[37] R.M. de Deugd, R.B. Chougule, M.T. Kreutzer, F.M. Meeuse, J. Grievink, F. Kapteijn, J.A. Moulijn, Is a monolithic loop reactor a viable option for Fischer–Tropsch synthesis?, Chem. Eng. Sci. 58 (2003) 583-591.

[38] C.A. Callaghan, Kinetics and Catalysis of the Water-Gas-Shift Reaction: A Microkinetic and Graph Theoretic Approach Department of Chemical Engineering Worcester Polytechnic Institute 2006.

[39] W.E.S. R. Byron Bird, Edwin N. Lightfoot Transport Phenomena, Revised Second Edition ed., Wiley 2012.

LIST OF FIGURES

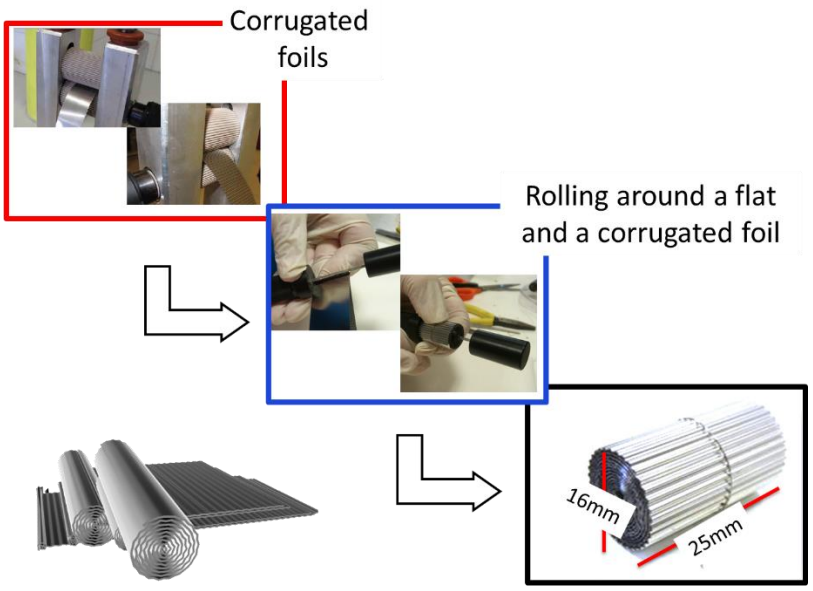

Figure 1. Manufacture and preparation of cylindrical metallic monolith

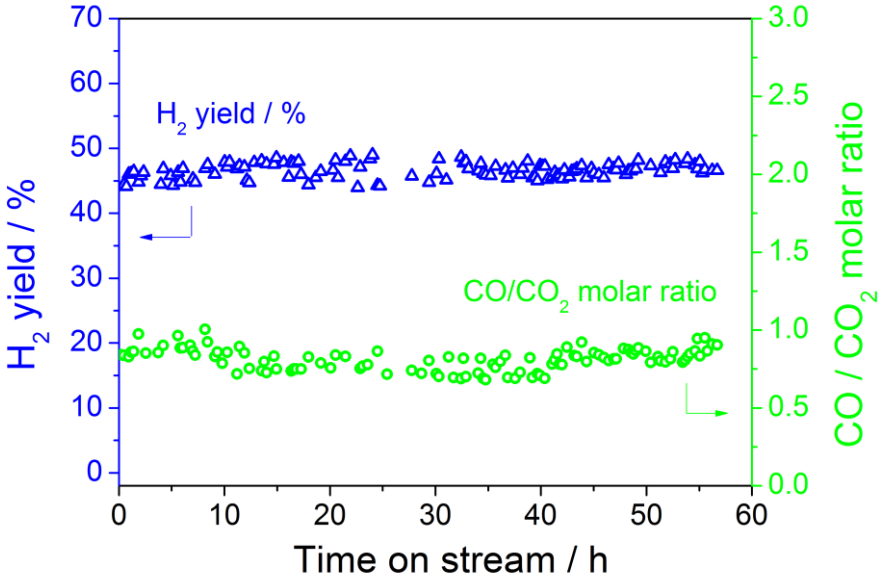

Figure 2. Hydrogen molar yield and CO/CO_2 molar ratio as function of time-on-stream. Reaction conditions: 750 ºC, 100 NL g^{-1} h^{-1}, atmospheric pressure, steam-to-carbon molar ratio = 4

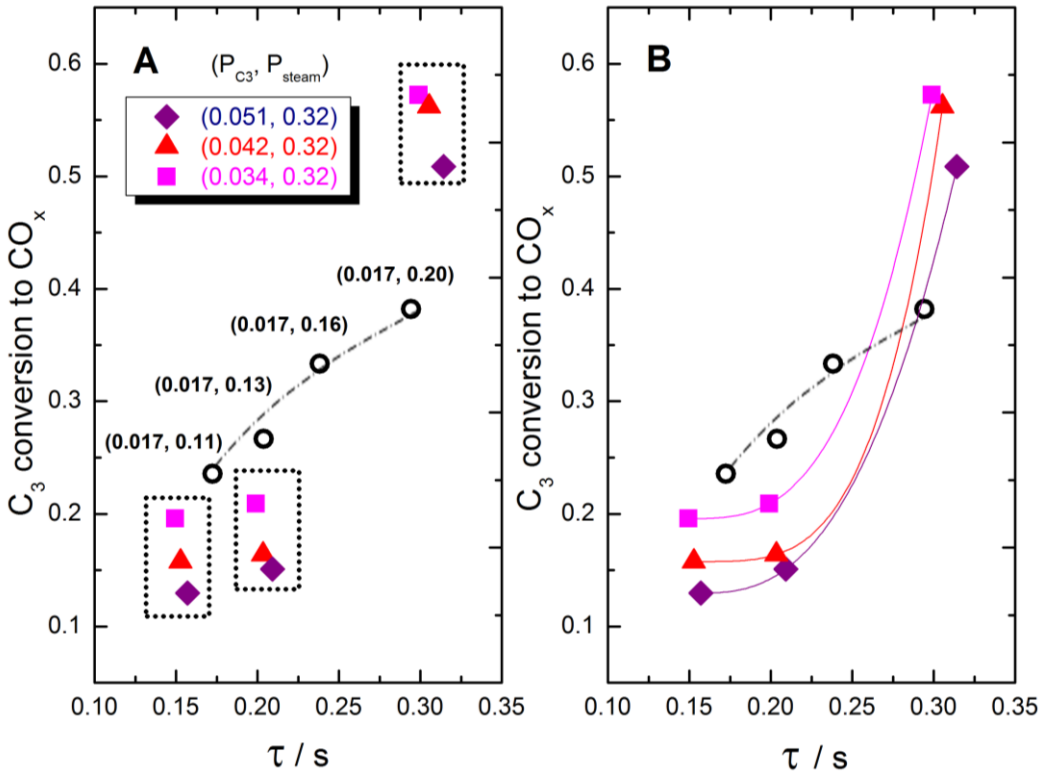
A
(P$_{C3}$, P$_{steam}$)
(0.051, 0.32)
(0.042, 0.32)
(0.034, 0.32)
(0.017, 0.20)
(0.017, 0.16)
(0.017, 0.13)
(0.017, 0.11)
C$_3$ conversion to CO$_x$
τ / s
B
C$_3$ conversion to CO$_x$
τ / s

Figure 3. Selected trends in glycerol initial conversion to steam reforming products as a function of space time and glycerol - steam partial pressures (atm) in the feed at T = 600 °C and P = 1 atm.

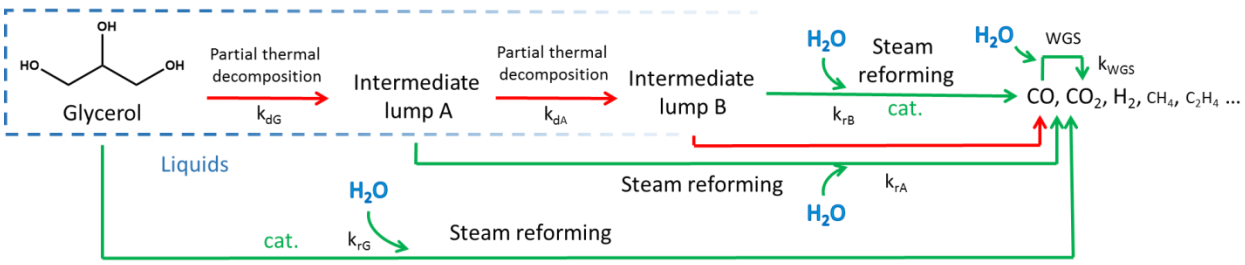

Figure 4. Sequential reaction scheme proposed for glycerol steam reforming

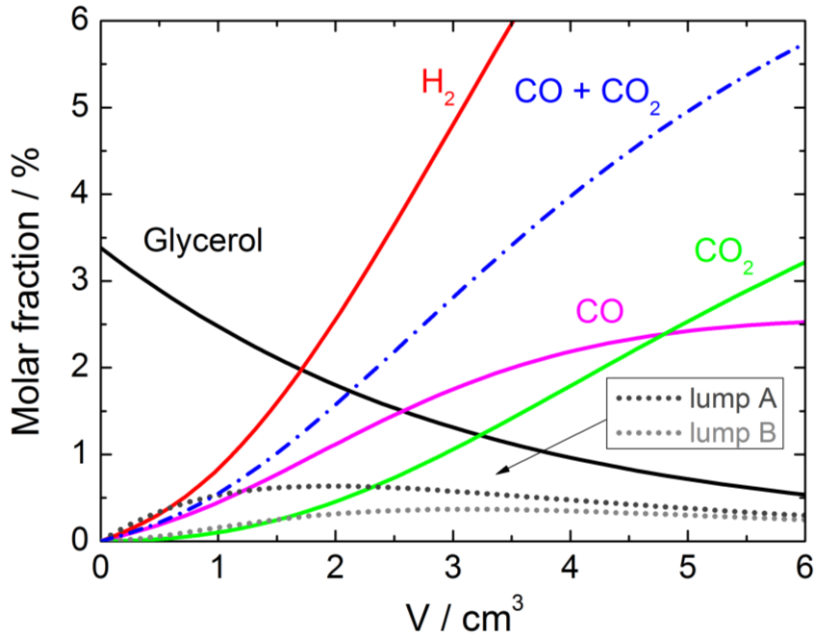
Molar fraction / %
V / cm3
H2
CO + CO2
Glycerol
CO2
CO
lump A
lump B
0
1
2
3
4
5
6

Figure 5. Selected ~~S~~simulated product yields according to primary + secondary + tertiary scheme in Fig. 4 (manually set parameters, in mol s^{-1} atm^{-1} m^{-3}: k_{dG} = 75, k_{rG} = 10, k_{dA} = 200, k_{rA} = 10, k_{rB} = 300; k_{WGS} = 432; p_{G0} = 0.034 atm, T = 600 °C)

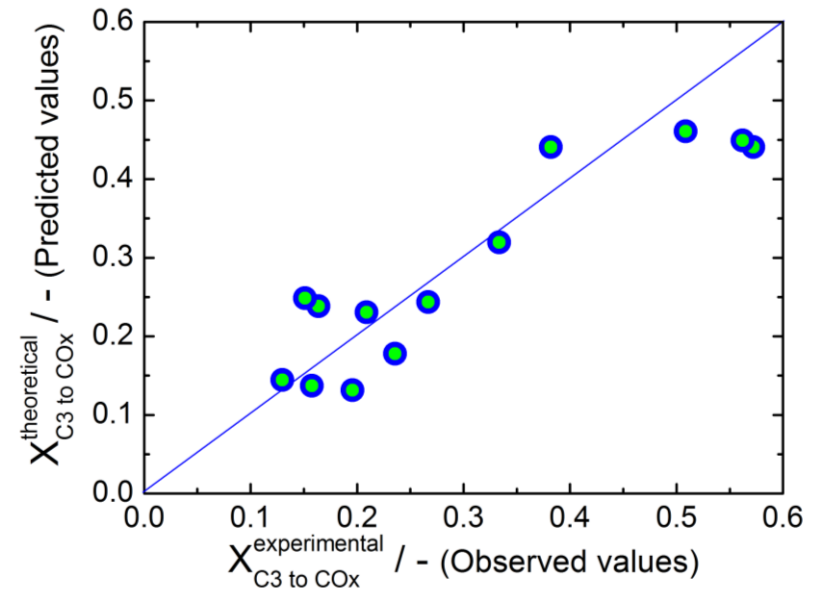

Figure 6. Parity plot of glycerol conversion for the adjusted parameters in Fig. 2 scheme (least-squares parameters, in mol s^{-1} m^{-3} atm^{-1}: k_{dG} = 105, k_{rG} = 0, k_{dA} = 125, k_{rA} = 0, k_{rB} = 124; k_{WGS} = 432 mol s^{-1} m^{-3} atm^{-2})

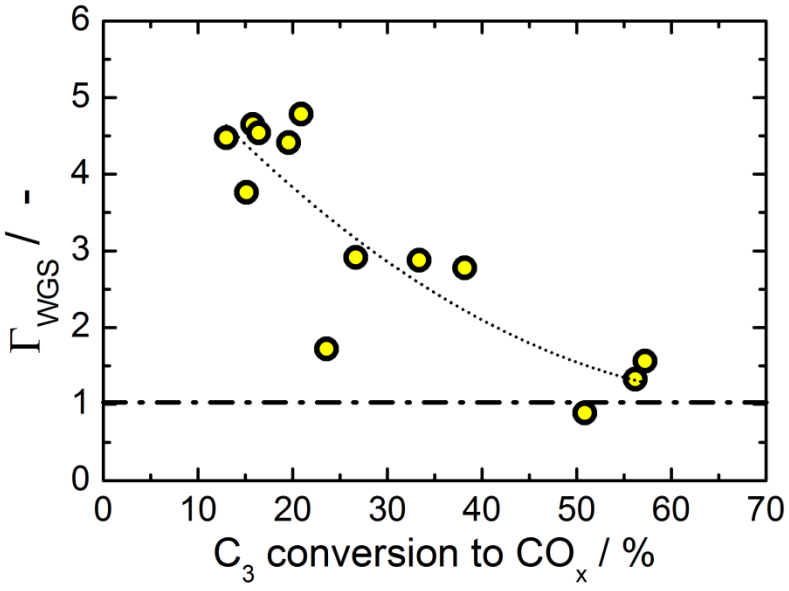

Figure 7. Approach to equilibrium in the WGS reaction as a function of the extent of glycerol steam reforming.

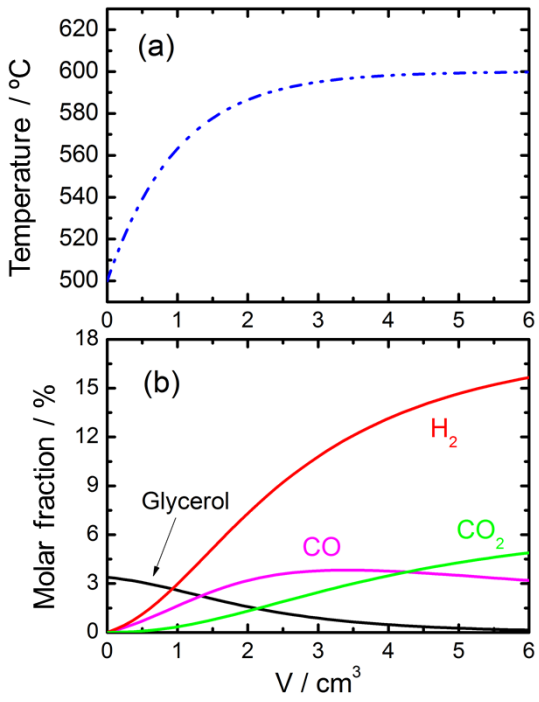

Figure 8. Effect of limited preheating on pseudohomogeneous first-order kinetics with respect to glycerol: (a) temperature profile, (b) main product distribution (k_{dG} (873.15 K) = 200 mol s^{-1} m^{-3} atm^{-1}, E_{adG} 110 kJ mol^{-1}, k_{WGS} = 432 mol s^{-1} m^{-3} atm^{-2}, p_{G0} = 0.034 atm, κ = 1 cm^{-3}, T_0 = 500 °C)

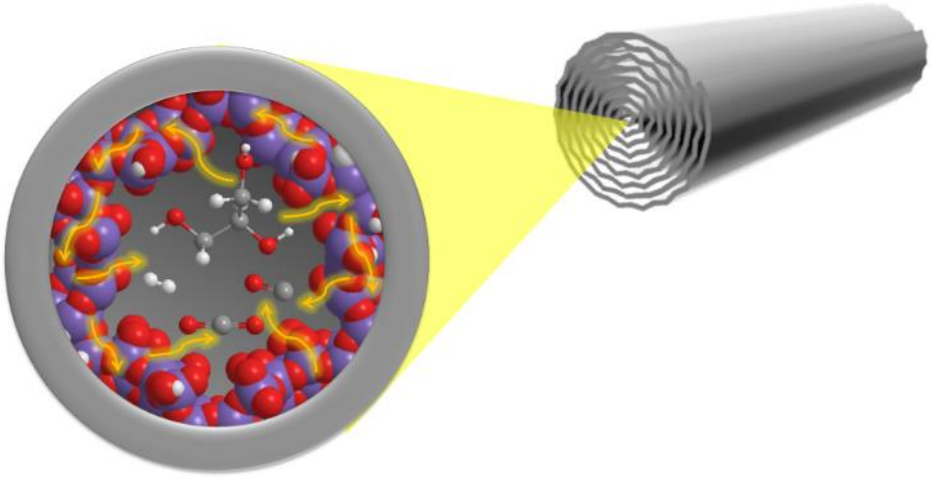

Figure 9. Diffusion and counterdiffusion to and from the monolith surface